PAPER

Check for updates

High-performance piezoelectric energy harvesting of vertically aligned Pb(Zr,Ti)O₃ nanorod arrays†

Wenchao Jin,[a] Zhao Wang, [ID] *[a] Hao Huang,[a] Xiaokang Hu,[b] Yahua He,[a] Meng Li,[a] Luying Li,[b] Yihua Gao, [ID] [b] Yongming Hu [ID] [a] and Haoshuang Gu*[a]

Recent developments of self-powered devices and systems have attracted much attention. Lead zirconate titanate (PZT) has been regarded as one of the most promising materials for building high-performance nanogenerators. Herein, vertically aligned PZT nanorod arrays were synthesized on a pre-oxidized Ti substrate in the presence of a surfactant by a one-step hydrothermal method. The PZT nanorod arrays consist of an initial layer of a PZT film and well aligned nanorods with (001)-orientated tetragonal single crystalline structures. The PZT nanorods exhibited a high piezoelectric response with a d_{33} value of up to 1600 pm V⁻¹. A piezoelectric energy harvester was fabricated based on the PZT nanorod arrays, which exhibited outstanding energy harvesting performance with an open-circuit output voltage of 3.3 V and 8 V when the devices were pressed by a compressive 10 N force and a finger tapping motion, respectively. Moreover, the average power density generated by those two mechanical stimulations were up to 3.16 and 5.92 μW cm⁻² with the external load of 1 MΩ.

Introduction

Rapid development of micro and nano-electronic technology has promoted the research and application of multi-functional personal electronics, wearable devices and smart sensor systems, *etc.*[1,2] Although the power consumption of such devices and systems has been reduced to a much lower level, the problem of long-term power supply in such miniaturized systems is still limiting their further development and application.[3,4] For instance, the dying battery has become one of the most serious puzzlements of smart phone users. Moreover, the recharging of sensor batteries used in untraversed environments such as underwater or enclosed conditions may also be a great challenge to engineers. Therefore, the research and development of novel types of electrical powering units with miniaturized dimensions, long lifetimes, good long-term stabilities but no recharging problems has become an attractive topic.

In recent years, the energy harvesters based on the photovoltaic, thermoelectric, electrochemical and piezoelectric effects have attracted great attentions due to their capability to convert the optical, thermal, chemical and mechanical energies into electrical output.[5–8] Such devices can be utilized for building the self-powered systems, which can independently operate by harvesting the energies in the ambient environment without any external electrical powering systems. Among the various kinds of energies, the mechanical energies such as the air flow, vibration and object movement have wide distributions and low limitation by the environmental conditions, which can be harvested and converted into electricity by using piezoelectric materials.[9–15]

Z. L. Wang's group firstly reported the micro-scaled piezoelectric energy harvester based on ZnO nanowire arrays in 2006.[16] After that, several kinds of nanowire-based energy harvesters have been demonstrated, including GaN, BaTiO₃, (K,Na)NbO₃ (KNN) and Pb(Zr,Ti)O₃ (PZT) nanowires.[12,17–23] Among them, PZT exhibited much better piezoelectric performance than other materials, including high piezoelectric constant (d_{33}) and electromechanical coupling coefficient.[24–31] For example, Chen *et al.* has demonstrated a piezoelectric energy harvester based on the electrospun PZT nanofibers with output voltage of 1.6 V.[25] However, the random alignment of the nanofibers limited the output performance of those devices. By integrate the PZT nanofibers into vertically aligned nanofiber arrays, Gu *et al.* obtained an ultra-high output piezoelectric energy harvester with output voltage of 209 V.[27]

Comparing with the polycrystalline nanofibers, the single-crystal nanowires always exhibited much better piezoelectric performance.[32] Lin and co-authors have demonstrated a hydrothermal growth of [110]-oriented vertically aligned PZT nanowire arrays on TiO₂ film.[33] However, there are no further

[a]Hubei Collaborative Innovation Center for Advanced Organic Chemical Materials, Hubei Key Laboratory of Ferro & Piezoelectric Materials and Devices, Faculty of Physics & Electronic Sciences, Hubei University, Wuhan, 430062, P. R. China. E-mail: wangzhao@hubu.edu.cn; guhsh@hubu.edu.cn

[b]Center for Nanoscale Characterization and Devices, Wuhan National Laboratory for Optoelectronics, Huazhong University of Science and Technology, Wuhan, 430074, China

† Electronic supplementary information (ESI) available. See DOI: 10.1039/c7ra13506h

investigation on the piezoelectric property of the nanowire arrays. Moreover, Xu *et al.* has reported a piezoelectric energy harvester based on the chemical epitaxially grown PZT nanowire array on $SrTiO_3$ (STO) single-crystal substrates in 2010.[28] However, the output voltage of such devices is lower than 1.0 V, which is much lower than the nanofiber-based devices and shows no obvious superiority than the other kinds of piezo-electric materials such as ZnO and $BaTiO_3$.[18,23,34] After that, few reports have been focused on either the synthesis or the piezoelectric performance of the single-crystal PZT nanowire arrays, limiting the application of these excellent piezoelectric materials in the micro-scaled energy harvesting devices.

In this work, vertically aligned single-crystal PZT nanorod arrays (NRAs) were synthesized on a pre-oxidized titanium foil by poly(vinyl alcohol) (PVA)-assisted hydrothermal process. The as-synthesized [001]-oriented PZT nanorods exhibited high piezo-electric constant up to 1600 pm V^{-1}. The as-fabricated vertically aligned nanogenerator (VING) exhibited outstanding energy harvesting performance with open-circuit output voltage (V_{OC}) up to 3.3 V under the compressive force of 10 N. The maximal output power density can reach 3.16 μW cm^{-2} with an external load resistance of 1 MΩ. The outstanding energy harvesting perfor-mance of the PZT NRAs provides great potential for the appli-cation in building high-performance self-powered systems.

Experimental

The PZT NRAs were synthesized by hydrothermal method on a layer of titanium oxide, which was formed on the surface of a titanium foil after a thermal treatment at 600 °C in air for 5 min. All regents used in the hydrothermal process are analytic pure and bought from the Sinopharm company. Tetrabutyl titanate ($[C_4H_9O]_4Ti$), zirconium oxychloride ($ZrOCl_2 \cdot 8H_2O$), and lead acetate trihydrate ($Pb[CH_3COO]_3$) were used as starting materials, potassium hydroxide was used as a mineralizer, and PVA was used as additives. Firstly, 0.8168 g $[C_4H_9O]_4Ti$ was dissolved in 26 ml ethanol to form Ti^{4+} solution. Then 0.8379 g $ZrOCl_2 \cdot 8H_2O$ was dissolved in 30 ml deionized (DI) water to form Zr^{4+} solution. After being stirred for 10 min, the Ti^{4+} solution was then added into the Zr^{4+} solution and strongly stirred for 10 min to form a transparent mixed solution. The mixed solution was introduced into a 150 ml ammonia solution with concentration of 0.15 M drop by drop, which resulted in the co-precipitation of $Zr_{0.52}Ti_{0.48}O(OH)_2$ (ZTOH) after half an

hour's holding. The co-precipitation was then extracted by centrifugal for 6 times. Then $Pb[CH_3COO]_2$, KOH (5.611 g) and PVA (vary from 0.04 g to 0.10 g) were all added to form the final hydrothermal precursor solution with total volume of 50 ml. The concentration of $Pb[CH_3COO]_2$, ZTOH, and KOH were 0.1, 0.1 and 2 M, respectively. After that, the pre-treated Ti substrate with size of 5 mm × 5 mm was kept 5 cm above the bottom of the autoclave by a Teflon holder and exposed to solution in both surface. 80% volume was filled by adding DI-water to the precursor. Then, the autoclave was kept in 180 °C for 12 h. After cooling the autoclave naturally to room temperature, the substrate was taken out and washed by DI-water, and then dried in air for 6 h at 60 °C.

The morphology of samples was obtained by field-emission scanning electron microscopy (FE-SEM, JEOL JSM7100F). The lattice structure and selected-area electron diffraction (SAED) patterns were studied and characterized by the X-ray diffraction spectrometer (XRD, Bruker D8A25, CuKα, λ = 0.15406 nm) and high-resolution transmission electron microscopy (HRTEM, JEOL JEM 2010). The morphology and piezoelectric property were researched through the scanning probe microscopy (SPM) and piezo-response force microscopy (PFM, NT-MDT). The energy harvesting performance was measured by using the dynamic mechanical analyser (DMA, Mettler Toledo DMA1) and data acquisition card (DAQ, NI USB-6210).

Results and discussion

Fig. 1 shows the FE-SEM images of the as-synthesized PZT products with different contents of PVA additives in the hydrothermal precursors. As shown in Fig. 1(a), no nanorods was formed on the surface of the substrates with the PVA content of 0.10 g. The surface of the product was consisted of condensed film with column-like grains. Moreover, the samples which were not attached on the substrate were consisting of cubic and amorphous particles, as shown in Fig. 1S.† When the PVA contents were lower than 0.10 g, the product was consisted of aligned PZT nanorods standing on the surface of the substrates. With the PVA content decreasing from 0.08 to 0.04 g, the estimated average diameter of the nanorods was ∼200, 400 and 1180 nm, respectively. As reported, the growth of PZT nanorods should be attributed to the adsorption of PVA on the (100) faces of the tetragonal perovskite structures due to the hydrogen bond under the high alkaline hydrothermal
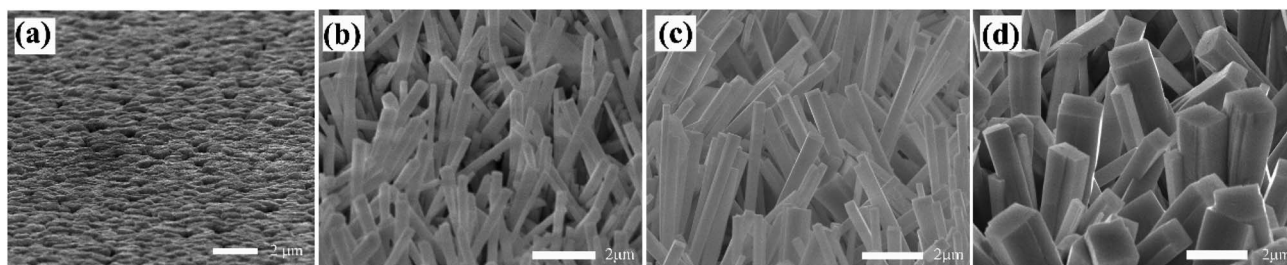

Fig. 1 The FE–SEM images of the products with different contents of PVA additives in the hydrothermal precursors. (a) 0.10 g; (b) 0.08 g; (c) 0.06 g; (d) 0.04 g.
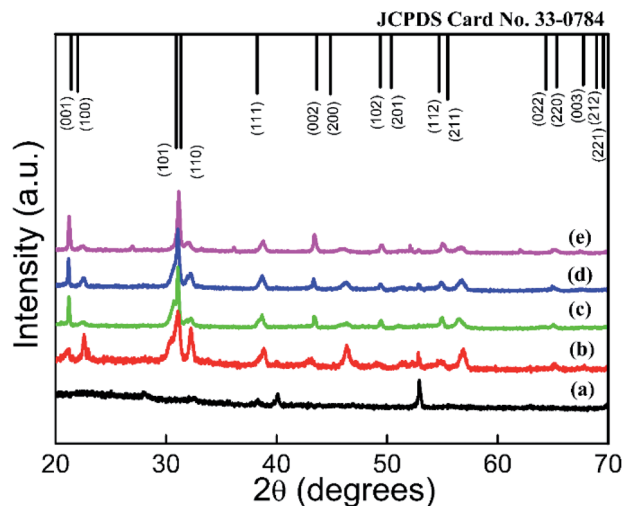
Fig. 2 The XRD pattern of the as-synthesized products with different PVA contents in the precursors. (a) Substrate; (b) 0.10 g; (c) 0.08 g; (d) 0.06 g; (e) 0.04 g.
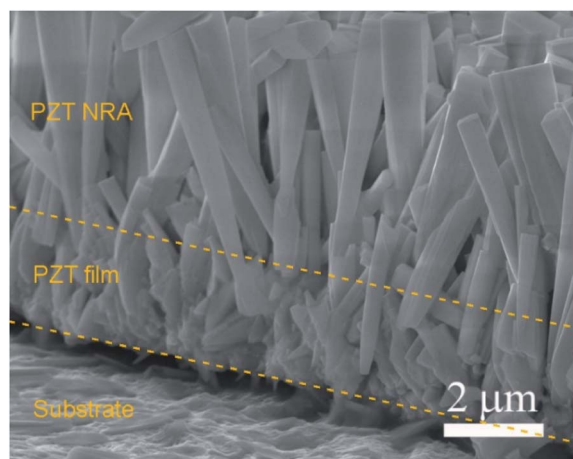

Fig. 3 The cross-section SEM image of the PZT NRAs with 0.1 g PVA.
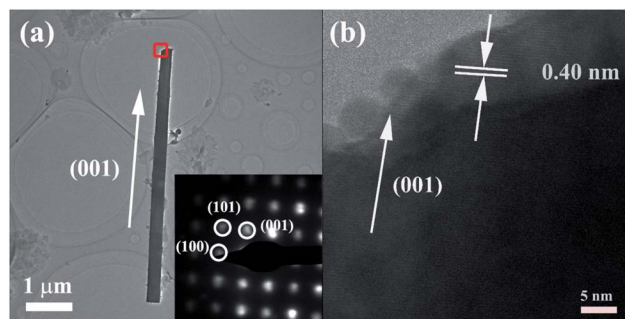

Fig. 4 The TEM results of the PZT nanorod with 0.08 g PVA. (a) TEM image and SAED patterns. (b) HRTEM image.

cross-section SEM image of the NRAs and the TEM characterization results.

As shown in Fig. 3, a layer of PZT film was formed at the initial stage of the hydrothermal process before the growth of the NRAs, which should be attributed to the reaction of the TiO_2 layer on the pre-treated Ti substrates with the hydrothermal precursors. Fig. 4 shows the TEM characterization of an individual PZT nanorod. According to the TEM image and the SAED pattern shows in Fig. 4(a), the PZT nanorod with ~200 nm in diameter and 6 μm in length exhibited single-crystalline tetragonal structure. The clear lattice fringes with spacing of 0.40 nm in the HRTEM image shown in Fig. 4(b), which corresponding to the red area in Fig. 4(a), confirmed the [001] growth orientation of the PZT nanorod, which agreed with the XRD results.

The radial piezoelectric response was measured by using PFM to evaluate the piezoelectric performance of the PZT nanorod. Firstly, the PZT nanorods were dispersed into ethanol and then transferred onto the surface of a piece of Au-coated silicon substrate. After been dried for 3 h at 60 °C, the sample was positioned onto the PFM holder to test the radial piezoelectric response of the nanorods. Fig. 5(a) shows a three-dimensional (3D) topography of an individual PZT nanorod, which is 2–3 μm in length and 200 nm in diameter, respectively. As shown in Fig. 5(b), the nanorod exhibited obvious symmetrical butterfly-shaped piezoelectric response loop, with maximum deformation of ~600 pm under bias of 1.5 V. The phase loop along with abrupt changes is shown in Fig. 5(c), in which the intensive peak at ~0.3 V was induced by a noise signal during the testing process. The results confirmed the spontaneous polarization behaviour of the PZT nanorod. Fig. 5(d) shows the piezo-response obtained as $M = A \cos \theta$, where M, A and θ represented the piezo-response, amplitude and phase angle, respectively. According to these curves, the maximum deformation was ~600 pm with phase switching of 180°. In addition, the piezoelectric constant could be calculated from the slope of the liner region of the curve. After the calibration by using a standard sample of $LiNbO_3$ with a nominal d_{33} value of 17.3 pm V^{-1}, the average piezoelectric constant d_{33} could be calculated to be ~1600 pm V^{-1}.[36,37] The much higher d_{33} of PZT nanorods suggested their high superiority in building piezoelectric energy harvesters than the ZnO, $BaTiO_3$ nanowires.

condition, which can suppress the growth of the adsorbed surface.[35] As a result, the decrease of PVA content may lower down the limitation of the growth along the radial direction, resulting in the increase of the diameter of the nanorods.

Fig. 2 shows the XRD patterns of the as-synthesized PZT products. All diffraction peaks can be indexed to the tetragonal perovskite phase of PZT and agree with the diffraction data of $PbZr_{0.52}Ti_{0.48}O_3$ in JCPDS card no. 33-0784. The sharp peaks indicate that the samples are well crystallized. The diffraction peaks at 27.4° belongs to the (110) face of TiO_2 layer on the substrate according to the JCPDS card no. 21-1276, while peaks at 25.1° and 53° belong to the (100) and (102) faces of the Ti substrate according to the JCPDS card no. 65-9622, respectively. Moreover, the intensity ratio between the (001) and (100) peaks of PZT was increased when the PVA content was decreased from 0.10 to 0.04 g. The results suggested the [001]-oriented growth of the PZT NRAs on the film, which could be further proved by the
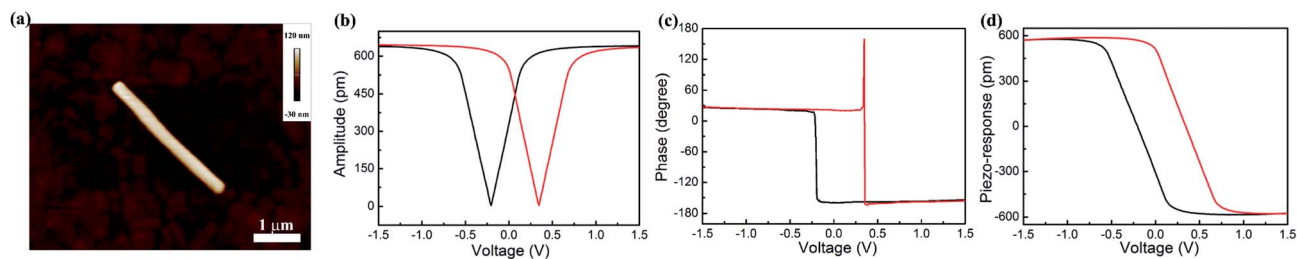
Fig. 5 The piezoresponse of PZT nanorod obtained with 0.08 g PVA. (a) The AFM morphology; (b) the amplitude curve; (c) the phase curve; (d) the piezoresponse curve.
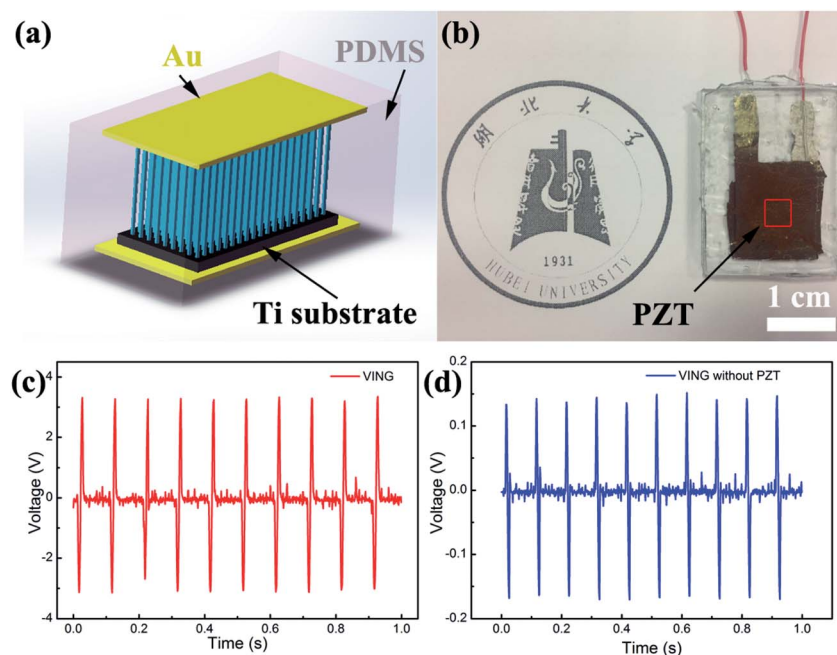

Fig. 6 The (a) schematic diagram, (b) photo image and (c and d) output voltage signal generated by harvesting the mechanical energy when the devices were vertically pressed by periodical tapping.

Fig. 6(a and b) show the schematic diagram and an optical photo image of the energy harvester based on the PZT NRAs. After the hydrothermal growth of the NRAs, a thin layer of PMDS was spin-coated to fill the interspace of the NRAs. Then a layer of Au electrodes of 100 nm in thickness was deposited on the top surface of the coated NRAs. After wire-leading, the whole device was packaged by the PDMS polymer to prevent the piezoelectric materials from physical damage and chemical interference. An outstanding energy harvesting performance can be observed when the device is subject to the axial pressure. According to the piezoelectric theory, the piezoelectric crystal under strain state will generate a piezoelectric field along the polarization direction, which will lead to a transient flow of free electrons in the external circuit to compensate the piezoelectric potential. Thus, an impulsive output voltage signal will be detected. In order to evaluate the device performance, a compressive force with constant amplitude of 10 N and frequency of 10 Hz was applied by using DMA in compressive

mode. As shown in the Fig. 6(c), the PZT NRA-based energy harvester can generate high electrical output with V_{OC} up to 3.3 V. Moreover, much higher open-circuit voltage (up to 8 V) can be generated when the device was knocked by human fingers (as shown in Fig. 2S†). To further confirm that PZT nanorods is the origin of the energy harvesting behaviour, a similar device without PZT NRAs but only the substrate and packaging layers was also fabricated. It can be seen in Fig. 6(d) that the device without PZT nanorods could generate much lower output voltage with amplitude of 0.14 V, which could be attributed to the release of electrostatic charges due to the capacitance effect of the devices. Therefore, the output voltage generated by the PZT-based devices could mainly be attributed to piezoelectric effect of PZT NRAs.

It is well accepted that the property of a power device lies on the capacity for driving the external loads. Fig. 7(a) shows the detected voltage signal applied on the external load resistance, which was varying from 10 kΩ to 1 GΩ. The voltage amplitude
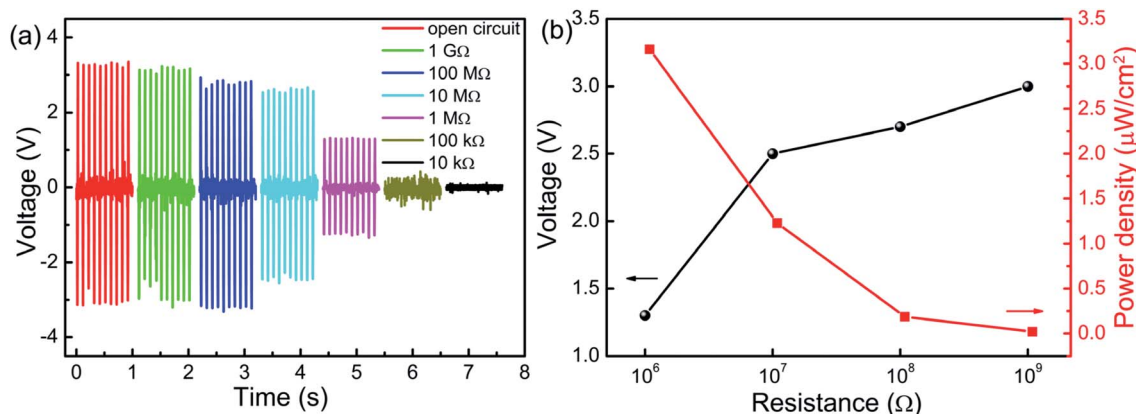
Fig. 7 (a) The voltage derived under different load resistance. (b) The variation of open-circuit output voltage and average power density with the load resistance.

Table 1 The comparison of output performance of the PZT-related nanogenerators

Sample	V_{OC} (V)	Maximum power (μW)	Maximum power density	Mechanical stimulation	Reference
Single PZT nanofiber	0.65	—		Bending by nanomanipulator	24
PZT nanofibers	1.63	0.03	—	Strain of 10% at 250 rad s^{-1}	25
PZT nanofiber arrays	209	—	—	Free-falling object	27
PZT NRAs	0.7		2.8 mW cm^{-3}	1–50 Hz	28
PZT ribbons	0.25	0.01		Finger tapping	39
PZT NRAs	3.3	0.79	3.16 μW cm^{-2}	Compressive force of 10 N at 10 Hz	This work
	8	1.48	5.92 μW cm^{-2}	Finger tapping	

increased with the increasing load resistance. However, the signal is unrecognizable when the resistance is lower than or equal to 100 kΩ, which should be attributed to the high internal resistance of the energy harvesters ($\sim$3 MΩ). Fig. 7(b) shows the average voltage and power density of the devices with varying load resistance under the applied force of 10 N. The average power density (P_L) was calculated according to the method reported by the previous works[25,38] as

$$P_L = \frac{1}{T} \int \frac{V_O(t)^2}{R_L} dt$$

where T is the time period (0.1 s), R is the load resistance and $V_O(t)$ is the output voltage, respectively. As shown, the peak of output voltage can reach $\sim$3 V when the resistance is 1 GΩ. The highest average power density was $\sim$3.16 μW cm^{-2} when the resistance is 1 MΩ. Moreover, Fig. 3S† shows the output performance of the devices under finger tapping. The highest V_{OC} was up to $\sim$8 V, while the average power density was up to $\sim$5.92 μW cm^{-2} with the resistance of 1 MΩ. Table 1 lists the reported works about the PZT-based nanogenerators. The device in this work shows higher open-circuit voltage than most of the devices in the previously reported works except the device basing on the nanofiber arrays with integrated electrical output. The outstanding energy harvesting performance with high output voltage and power density indicated the great potential of the PZT NRAs for the application of high-

performance piezoelectric energy harvesters and self-powered systems.

Conclusions

In this work, aligned PZT NRAs with high aspect ratio and uniform distribution were synthesized on pre-oxidized Ti substrates by using a hydrothermal method. The polymer surfactant plays a vital role in the size and morphology of the arrays. The nanorods were confirmed to be the (001) oriented with single-crystal tetragonal perovskite structure. The NRs exhibit high piezoelectric constant along the radial direction, which is $\sim$1600 pm V^{-1}. The energy harvesters based on the PZT NRAs could generate impulsive voltage with open-circuit value up to 3.3 V when the device was vertically pressed by a compressive force of 10 N at 10 Hz. The average output power density was up to 3.16 μW cm^{-2} when the load resistance is 1 M. Those output performance parameters were increased to 8 V and 5.92 μW cm^{-2} when the devices were knocked by a human finger. The outstanding energy harvesting performance of the PZT NRAs can provide many opportunities for the application of self-powered nano-devices and systems.

Conflicts of interest

There are no conflicts to declare.

Acknowledgements

Notes and references

1 W. Wu, X. Wen and Z. L. Wang, *Science*, 2013, **340**, 952.
2 S. Lee, S.-H. Bae, L. Lin, Y. Yang, C. Park, S.-W. Kim, S. N. Cha, H. Kim, Y. J. Park and Z. L. Wang, *Adv. Funct. Mater.*, 2013, **23**, 2445.
3 H. A. Sodano, D. J. Inman and G. Park, *J. Intell. Mater. Syst. Struct.*, 2005, **16**, 799.
4 N. Elvin, A. Elvin and D. H. Choi, *J. Strain Anal. Eng. Des.*, 2003, **38**, 115.
5 M. Grätzel, *Inorg. Chem.*, 2005, **44**, 6841.
6 D. Liang, H. Yang, S. W. Finefrock and Y. Wu, *Nano Lett.*, 2012, **12**, 2140.
7 H. Yang, L. A. Jauregui, G. Zhang, Y. P. Chen and Y. Wu, *Nano Lett.*, 2012, **12**, 540.
8 Y. Gogotsi and P. Simon, *Science*, 2011, **334**, 917.
9 Z. L. Wang and W. Wu, *Angew. Chem., Int. Ed.*, 2012, **51**, 11700.
10 Y. Hu, Y. Zhang, C. Xu, G. Zhu and Z. L. Wang, *Nano Lett.*, 2010, **10**, 5025.
11 Y. Hu, L. Lin, Y. Zhang and Z. L. Wang, *Adv. Mater.*, 2012, **24**, 110.
12 Y. He, Z. Wang, X. Hu, Y. Cai, L. Li, Y. Gao, X. Zhang, Z. Huang, Y. Hu and H. Gu, *RSC Adv.*, 2017, 7, 16908.
13 M. Lee, J. Bae, J. Lee, C.-S. Lee, S. Hong and Z. L. Wang, *Energy Environ. Sci.*, 2011, **4**, 3359.
14 R. Yang, Y. Qin, L. Dai and Z. L. Wang, *Nat. Nanotechnol.*, 2009, **4**, 34.
15 C. Chang, V. H. Tran, J. Wang, Y. K. Fuh and L. Lin, *Nano Lett.*, 2010, **10**, 726.
16 Z. L. Wang and J. Song, *Science*, 2006, **12**, 242.
17 N. Jamond, P. Chrétien, L. Gatilova, E. Galopin, L. Travers, J. Harmand, F. Glas, F. Houzé and N. Gogneau, *Nanoscale*, 2017, **9**, 4610.
18 A. Koka, Z. Zhou and H. A. Sodano, *Energy Environ. Sci.*, 2014, **7**, 288.
19 W. S. Su, Y. F. Chen, C. L. Hsiao and L. W. Tu, *Appl. Phys. Lett.*, 2007, **90**, 063110.
20 X. Wang, J. Song, F. Zhang, C. He, Z. Hu and Z. Wang, *Adv. Mater.*, 2010, **22**, 2155.
21 A. Koka and H. A. Sodano, *Adv. Energy Mater.*, 2014, **4**, 1301660.
22 C. Y. Chen, T. H. Liu, Y. Zhou, Y. Zhang, Y. L. Chueh, Y. H. Chu and Z. L. Wang, *Nano Energy*, 2012, **1**, 424.
23 A. Koka, Z. Zhou, H. Tang and H. A. Sodano, *Nanotechnology*, 2014, **25**, 375603.
24 X. Chen, S. Xu, N. Yao, W. Xu and Y. Shi, *Appl. Phys. Lett.*, 2009, **94**, 253113.
25 X. Chen, S. Xu, N. Yao and Y. Shi, *Nano Lett.*, 2010, **10**, 2133.
26 R. Guo, L. Cross, S. Park, B. Noheda, D. Cox and G. Shirane, *Phys. Rev. Lett.*, 2000, **84**, 5426.
27 L. Gu, N. Cui, L. Cheng, Q. Xu, S. Bai, M. Yuan, W. Wu, J. Liu, Y. Zhao, F. Ma, Y. Qin and Z. L. Wang, *Nano Lett.*, 2013, **13**, 91.
28 S. Xu, B. J. Hansen and Z. L. Wang, *Nat. Commun.*, 2010, **1**, 93.
29 S. Yang, M. Sanghadasa and S. Priya, *Nanotechnology*, 2013, **24**, 225303.
30 X. Zhang, X. Zhao, C. Lai, J. Wang, X. Tang and J. Dai, *Appl. Phys. Lett.*, 2004, **85**, 4190–4192.
31 Y. Chen, T. Liu, C. Chen, C. Liu, S. Chen, W. Wu, Z. Wang, J. He, Y. Chu and Y. Chueh, *ACS Nano*, 2012, **6**, 2826–2832.
32 X. Cui, X. Ni and Y. Zhang, *J. Alloys Compd.*, 2016, **675**, 306.
33 Y. Lin, Y. Liu and H. A. Sodano, *Appl. Phys. Lett.*, 2009, **95**, 122901.
34 G. Zhu, R. Yang, S. Wang and Z. L. Wang, *Nano Lett.*, 2010, **10**, 3151.
35 Y. Hu, H. Gu, D. Zhou, Z. Wang, H. L.-W. Chan and Y. Wang, *J. Am. Ceram. Soc.*, 2010, **93**, 609.
36 D. Staedler, T. Magouroux, R. Hadji, C. Joulaud, J. Extermann, S. Schwung, S. Passemard, C. Kasparian, G. Clarke, M. Gerrmann, R. Le Dantec, Y. Mugnier, D. Rytz, D. Ciepielewski, C. Galez, S. Gerber-Lemaire, L. Juillerat-Jeanneret, L. Bonacina and J. P. Wolf, *ACS Nano*, 2012, **6**, 2542–2549.
37 R. Weis and T. K. Gaylord, *Appl. Phys. A*, 1985, **37**, 191–203.
38 J. Briscoe, N. Jalali, P. Woolliams, M. Stewart, P. M. Weaver, M. Cain and D. Steve, *Energy Environ. Sci.*, 2013, **6**, 3035–3045.
39 Y. Qi and M. Mcalpine, *Energy Environ. Sci.*, 2010, **3**, 1275–1285.